Cold Regions Science and Technology 69 (2011) 139–144

Contents lists available at SciVerse ScienceDirect

Cold Regions Science and Technology

journal homepage: www.elsevier.com/locate/coldregions

Measurements of weak layer fracture energy

Jürg Schweizer [a,*], Alec van Herwijnen [a,b], Benjamin Reuter [a]

[a] WSL Institute for Snow and Avalanche Research SLF, Davos, Switzerland
[b] Department of Civil Engineering, Montana State University, Bozeman, MT, USA

ARTICLE INFO

Article history:
Received 8 January 2011
Revised 1 June 2011
Accepted 7 June 2011

Keywords:
Snow mechanical properties
Snow avalanche
Avalanche release
Fracture mechanics
Fracture energy

ABSTRACT

Dry-snow slab avalanches release by a sequence of fractures. The two main parameters which are initially of fundamental importance for the fracture process are the weak layer specific fracture energy and the stiffness of the overlying slab. So far, only few values of weak layer fracture energy exist, mainly because the stiffness of the slab cannot easily be determined. We have performed about 150 propagation saw tests to obtain the weak layer fracture energy from measurements of critical crack length, slab thickness and density. To estimate the stiffness of the slab needed to calculate the energy release rate, we used snow micro-penetrometer measurements. The values of the effective elastic modulus ranged from 1.8 to 12 MPa. The specific fracture energy of the weak layer was evaluated using a finite element (FE) model. For our weak layer/slab configurations we obtained specific fracture energies on the order of 1 J m^{-2}. These values are large compared to the only previously published value based on field measurements of 0.07 J m^{-2}. However, comparison with an independent approach using a video sequence of one fracture test confirmed our results. Many more measurements are needed for a comprehensive dataset of weak layer fracture energy.

1. Introduction

The release of a dry-snow slab avalanche can be envisaged as a fracture process (McClung, 1979, 1981). It is believed to start with the failure in a weak layer below a cohesive slab. This initial failure has to grow to a critical size, the size when the crack becomes self-propagating. The resistance to crack propagation can be described by the fracture toughness or the fracture energy. Assuming linear elastic behavior, the energy available for crack growth is given by the rate of change in potential energy with crack area and is called the energy release rate. At the critical crack size, the energy release rate corresponds to the specific fracture energy of the weak layer — a measure of toughness. The second important material property is the slab stiffness as is determines how much energy can be released to drive fracture. The energy release rate is inversely proportional to the modulus of the slab (Anderson, 1995). As the crack becomes self-propagating, the weak layer collapses releasing gravitational potential energy (Jamieson and Schweizer, 2000). Recent theoretical and experimental results suggest that this collapse plays an important role in the release of dry-snow slab avalanches (Heierli et al., 2008; van Herwijnen et al., 2010).

The specific fracture energy and the stiffness of the overlying slab are therefore of fundamental importance and the relevant properties of snow to be measured if fracture mechanical models for avalanche release should become applicable. Sigrist and Schweizer (2007) provided the first values of fracture energy derived from field measurements. Using a similar design for the field test as Gauthier and Jamieson (2006) to determine the critical cut length, they used a finite element (FE) model to determine the weak layer fracture energy. The elastic modulus of the slab that is required to calculate the fracture energy was derived from in-situ penetration resistance measurements using a snow micro-penetrometer (SMP) (Schneebeli and Johnson, 1998). For a persistent weak layer consisting of mainly faceted crystals and some depth hoar (1–2 mm in size) Sigrist and Schweizer (2007) reported a critical energy release rate (or weak layer fracture energy) of $0.07 \pm 3.10.02$ J m^{-2}. The overlying slab was 26 cm thick (slope perpendicular) and had an average density of 187 kg m^{-3}.

Similarly, Gauthier (2007) derived fracture energies from a large data set of propagation saw test results based on the work by Sigrist (2006). Assuming a homogeneous slab layer Sigrist (2006) had provided an approximate analytical solution for determining the critical energy release rate based on an analytical model for collapse in horizontal stratifications (Heierli and Zaiser, 2006). To determine the critical energy release rate, Gauthier (2007) used this approximate analytical solution together with an empirical relation for the density dependence of the elastic modulus (Sigrist, 2006). He reported a median critical energy release rate of 0.3 J m^{-2}, with an interquartile range of 0.15–0.5 J m^{-2} — about an order of magnitude larger than Sigrist's (2006) analytical values. The slab layers in Gauthier's (2007) field tests tended to be thicker and denser than in Sigrist's (2006) field tests, whereas the critical crack lengths were similar. A

* Corresponding author at: WSL Institute for Snow and Avalanche Research SLF, Flüelastrasse 11, CH-7260 Davos Dorf, Switzerland. Tel.: +41 81 4170164; fax: +41 81 4170110.
E-mail address: schweizer@slf.ch (J. Schweizer).

0165-232X/$ – see front matter © 2011 Elsevier B.V. All rights reserved.
doi:10.1016/j.coldregions.2011.06.004

recent re-analysis of Gauthier's (2007) field tests revealed that the values reported were too high by about a factor of 8 due to a calculation error stemming from missing brackets in one of the equations in Sigrist's (2006) thesis (Gauthier and Jamieson, 2010).

Similarly low values for the critical energy release rate have been reported in a number of preceding – mainly laboratory – studies (e.g. Kirchner et al., 2000; Schweizer et al., 2004; Sigrist et al., 2006). In addition, McClung (2007) has derived fracture energies from field measurements taken at fracture lines of snow slab avalanches and suggested a range for the critical energy release rate of alpine snow in mode II of 0.001–0.2 J m^{-2}.

Whereas Sigrist (2006) only considered the slope normal displacement for his approximate analytical solution of the energy release rate, Heierli (2008) subsequently derived a more comprehensive analytical solution which considers all terms contributing to the mechanical energy. Consequently, as most of the additional terms are positive, larger values of the fracture energy (than obtained with the approximate solution used by Sigrist (2006)) result.

The above reported low values of the specific fracture energy have never been confirmed by an independent measurement method. In any case, the values are highly sensitive to the assumptions made when the elastic modulus of the slab is determined. Furthermore, thus far there is no dataset with values of the specific fracture energy for various types of weak layers.

Recently, van Herwijnen and Heierli (2010a,b) proposed an alternative method for determining the critical fracture energy. They analyzed the deformation field as obtained from a video sequence of the fracture experiments with particle tracking velocimetry (PTV). From the measured amount of bending they derived an average elastic modulus for the slab, and independently thereof the weak layer fracture energy. This method, which we will call PTV method, allows one to verify the values of the modulus derived from the SMP signal.

The aim of the present study is to provide additional values of specific fracture energy for different types of weak layers based on field experiments using the propagation saw test. Based on an improved geometry for the FE model and a recently developed algorithm to extract the modulus from the SMP signal (Marshall and Johnson, 2009), we assess typical slab configurations, compare the analytical with the numerical method, provide new values for the fracture energy of weak layers determined with the SMP-FE method, and finally compare those with the result from one experiment using the PTV method.

2. Methods

During the winter 2009–2010 we performed about 150 propagation saw tests (PST) on eight slopes above tree line near Davos (Eastern Swiss Alps) (Table 1). The block length was always at least 120 cm, the cut direction was always up-slope and the top and bottom end faces of the blocks were cut slope normal. Otherwise we followed the procedures for the PST as described in Gauthier and Jamieson (2006). Measurements included the critical cut length, slab thickness and slope angle. A nearby snow profile provided slab and weak layer stratigraphy and layer density. All tests were completed with snow micro-penetrometer (SMP) measurements (Schneebeli and Johnson, 1998) in order to obtain the detailed layering at the test location and to derive the modulus from penetration resistance (see below). On one occasion (12 March 2010) we also recorded a video sequence of the fracture test.

Table 1
Date, location and characteristics of slopes with *N* number of propagation saw tests performed.

Date	Location	Slope angle (°)	Elevation (m a.s.l.)	Aspect	*N*
8 Feb 2010	Chilcherberg	20	2410	SE	19
15 Feb 2010	Hüreli	20	2200	S	15
16 Feb 2010	Steintälli	30	2430	E	18
25 Feb 2010	Steintälli	30	2400	S	18
3 Mar 2010	Dorfberg	33	2200	SE	14
8 Mar 2010	Vorder Latschüel	20	2480	SW	18
12 Mar 2010	Chilcherberg	30	2460	S	23
18 Mar 2010	Mittelgrat	29	2480	W	24

To determine the specific fracture energy of a weak layer the elastic properties of the slab need to be known. Three methods can in principal be applied to estimate those: (1) The modulus can be estimated solely based on density using a relation such as provided by Scapozza (2004) or Sigrist (2006). (2) The modulus can be evaluated from the SMP signal using an algorithm proposed by Johnson and Schneebeli (1999) and recently improved by Marshall and Johnson (2009); we will call this method the SMP method. (3) The modulus can be determined using the PTV method as suggested by van Herwijnen and Heierli (2010a). We will use the first two methods, and in one instance compare our results with those van Herwijnen and Heierli (2010a) obtained with the PTV method.

For the PTV method, the observed displacement (bending of the part of the block above the saw cut) is analyzed and the modulus is derived by either fitting the observed displacement field to the theoretical displacement, which can be obtained by assuming that the overhanging part of the block behaves like a Timoshenko beam, or by analyzing the change in mechanical energy with increasing cut length.

When determining the elastic modulus of the slab using the SMP method, the micro-modulus was obtained with the algorithm described by Marshall and Johnson (2009) which is the latest approach to the extraction of micromechanical properties from SMP data. The algorithm calculates the characteristic quantities of an SMP signal: mean rupture force, structural element length and deflection at rupture, and then determines the elastic modulus of microstructural elements. The latter describes the bending of snow grains before failure and is implemented as described by Sturm et al. (2004). We did not use a factor to fit the micro-modulus to observed values of the Young's modulus as previously done by Kronholm (2004) or Sigrist (2006), primarily since the algorithm we used (Marshall and Johnson, 2009) provided different values than the original algorithm used by Kronholm (2004). As our values were in the same range as those measured by Camponovo and Schweizer (2001), we deemed adjusting them unnecessary. Furthermore, we only used quality checked SMP signals for the analysis; signals that exhibited a significant drift or signs of a frozen sensor were discarded.

Once the elastic properties are estimated the specific fracture energy of the weak layer can be evaluated by either (a) using the analytical solution provided by Heierli (2008, Eq. 4.13) or (b) using a finite element model as described by Sigrist (2006) and Sigrist and Schweizer (2007); alternatively, the PTV method can be used (van Herwijnen and Heierli, 2010a).

Assuming that only the elastic strain energy of the overhanging part of the block (above the saw cut) changes, Heierli (2008) provided an expression for the total energy U of the configuration used in the field test:

$$U(r) = U_s + U_m = w_f dr - \frac{\pi\gamma dr^2}{4E}\left(\tau^2+\sigma^2\right) - \frac{dr^3}{6EH}\left(\lambda_1\tau^2+\lambda_2\tau\sigma+\lambda_3\sigma^2\right) \quad (1)$$

with U_s the crack surface energy, w_f the specific fracture energy, and U_m the mechanical energy. The second term on the right hand side is the fracture mechanical energy which is released if a crack of length r opens in a block of width d. The third term accounts for longer cracks and modified boundary conditions considering the slab as Timoshenko beam. Here H is the slab thickness, γ is a constant of about one, depending on Dundur's elastic mismatch parameter and E is the elastic modulus of the slab. The load on the undisturbed

weak layer consists of a shear stress $\tau = \rho g H \sin\alpha$ and a negative compressive stress $\sigma = -\rho g H \cos\alpha$ (Heierli, 2008). Furthermore,

$$\lambda_1 = 1 + \frac{9\eta H}{4r} + \frac{9\eta^2 H^2}{4r^2}, \lambda_2 = \frac{9\eta}{2} + \frac{9\eta^2 H}{2r}, \lambda_3 = 3\eta^2 + \frac{9\eta r}{4H} + \frac{9r^2}{5H^2} \quad (2)$$

with $\eta = \sqrt{4(1+\nu)/5}$ and ν the Poisson's ratio. According to the Griffith's fracture criterion r maximizes U at the equilibrium of the system. Thus, the determination of the specific fracture energy w_f reduces to the calculation of the extremum of U with respect to r ensuring that it is a maximum:

$$\frac{1}{d}\frac{dU(r)}{dr} = w_f + \frac{1}{d}\frac{dU_m}{dr} = 0. \quad (3)$$

Arranging the remaining terms for the calculation of the specific fracture energy according to the power of r/H yields:

$$w_f = \frac{H}{2E}\left[w_0 + w_1\frac{r}{H} + w_2\left(\frac{r}{H}\right)^2 + w_3\left(\frac{r}{H}\right)^3 + w_4\left(\frac{r}{H}\right)^4\right] \quad (4)$$

with

$$w_0 = \frac{3\eta^2}{4}\tau^2, \quad (5)$$

$$w_1 = \left(\pi\gamma + \frac{3\eta}{2}\right)\tau^2 + 3\eta^2\sigma\tau + \pi\gamma\sigma^2, \quad (6)$$

$$w_2 = \tau^2 + \frac{9\eta}{2}\sigma\tau + 3\eta^2\sigma^2, \quad (7)$$

$$w_3 = 3\eta\sigma^2, \quad (8)$$

$$w_4 = 3\sigma^2. \quad (9)$$

Because sawing from the lower end of the block leads to a negative shear stress ($\tau<0$; Heierli, 2008), all terms are positive. Assuming $H=0.3$ m, $E=3$ MPa, $\gamma=1$, $\nu=0.17$, $\rho=240$ kg m^{-3}, $\alpha=30°$ and $r=0.3$ m results in $w_f=0.34$ J m^{-2}. For short cut length ($r<H$) the terms w_1 and w_2 dominate, while for longer cut length ($r>2H$) the terms w_3 and w_4 become dominant.

With the finite element method, an analysis of the slab can consist of several layers with varying material properties, whereas an average modulus is used with the analytical solution. Therefore, with the FE method one can investigate more realistic slab configurations. We used Sigrist's (2006) finite element model implemented in the ANSYS workbench, to determine the critical energy release rate from the calculation of the elastic strain energy. We adapted the geometry of Sigrist's (2006) FE model to account for up-slope sawing and for slope normal front and end faces (Fig. 1). The model consisted of a base layer whose nodes were fixed at the bottom in the x-direction, a weak layer and up to seven slab layers. A preliminary sensitivity analysis revealed that the thickness of the base layer can considerably influence the calculated fracture energy values; for our geometry, deformation contributing to the energy release rate was observed up to a thickness of the basal layer of about 40 cm, about equivalent to the slab thickness. We therefore used a base (or substratum) thickness of 40 cm, which is thicker than used by Sigrist (2006). The thickness of the weak layer, which is still intact over the ligament length a (Fig. 1), was constant and the same as the gap width, i.e. 3 mm.

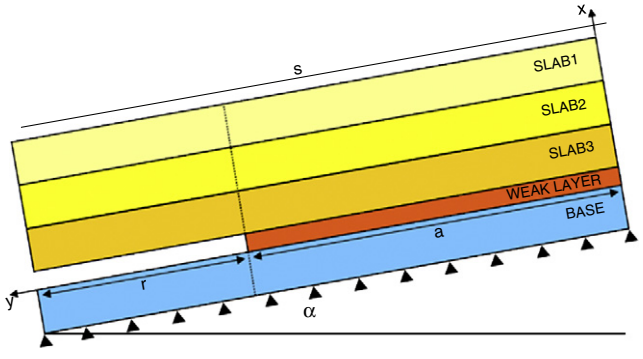

Fig. 1. Geometry of finite element (FE) model. α: slope angle, r: cut length, a: ligament length, s: length of block ($s=1.2$ m).

The thickness and properties of the slab layers were determined from the penetration resistance measurement. The density was taken from the nearby snow profile. The properties of the base layer were also derived from the SMP profile and the snow profile. The weak layer was modeled with the properties of the base layer as often thick weak layers were present.

The elastic strain energy is calculated by summing up the entries of all nodes of the slab, the weak layer and the base. The critical energy release rate G_c is determined from the change in elastic strain energy U_m for a small change in cut length $\delta r = 2$ mm at the critical cut length r_c:

$$G_c = \frac{1}{d}\frac{U_m(r_c+\delta r) - U_m(r_c)}{\delta r} \quad (10)$$

where d is the block width (Sigrist, 2006).

In order to assess the effect of the slab layering on the critical cut length for a given weak layer fracture energy, we used six different typical slab layer configurations (e.g. Habermann et al., 2008; Schweizer and Lütschg, 2001). The slab configurations are shown in Fig. 2 and the corresponding properties given in Table 2. Three layers (soft, medium, hard — based on density) with corresponding material properties were defined. To ensure comparability, the average slab thickness and density were kept constant (30 cm and 240 kg m^{-3}, respectively). Typical values of the effective modulus were chosen according to density (e.g. Mellor, 1975). Other model parameters were slope angle

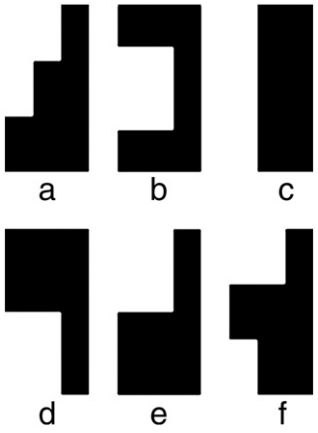

Fig. 2. Simplified slab configurations for sensitivity analysis.

Table 2
Material properties of slab layers for sensitivity analysis with simplified slab configurations consisting of three slab layers (Fig. 2).

Profile type	Layer thickness (cm)			Density (kg m^{-3})			Modulus (MPa)		
a	10	10	10	120	240	360	0.3	3	15
b	7.5	15	7.5	360	120	360	15	0.3	15
c	10	10	10	240	240	240	3	3	3
d	7.5	7.5	15	360	360	120	15	15	0.3
e	15	7.5	7.5	120	360	360	0.3	15	15
f	10	10	10	120	360	240	0.3	15	3

For each profile type three slab layers are defined. Total slab thickness was always 30 cm, average slab density was always 240 kg m^{-3}.

$\alpha = 30°$, block length $s = 1.2$ m, block width $d = 0.3$ m, gap width $\Delta_{gap} = 0.005$ m, thickness of base layer $h_{base} = 0.4$ m, density of base layer $\rho_{base} = 240$ kg m^{-3}, elastic modulus of the base $E_{base} = 3$ MPa. The weak layer had the same properties as the base. The values of the Poisson's ratio were estimated according to density as described by Sigrist and Schweizer (2007).

3. Results

3.1. FE sensitivity analysis and comparison with analytical solution

The sensitivity analysis for the numerical model with the six different slab configurations revealed that the shortest cut lengths resulted with hard layers on top of soft ones for a given weak layer fracture energy (Fig. 3). For example, for a specific fracture energy $w_f = 1$ J m^{-2} the critical cut length varied by almost a factor of 2 between 20 cm (profile d) and over 35 cm (profile e). The critical cut lengths were longest for slab configurations with hard layers just above the weak layer (profiles a and e).

For the standard test geometry and typical material properties, i.e. a uniform slab with $E_{slab} = 3$ MPa, the analytical solution was compared to the numerical results (FE) for different cut lengths (Fig. 4a). As the slope normal displacement (bending) of the overhanging part of the slab above the cut increased with increasing cut length, the energy release rate increased. The energy release rates obtained with the FE model were slightly larger than those calculated with the analytical solution if the base layer was assumed as relatively stiff ($E_{base} = 60$ MPa) compared to the slab layers ($E_{slab} = 3$ MPa). Using more realistic values for the properties of the base layer, the difference between the analytical and the numerical simulation increased.

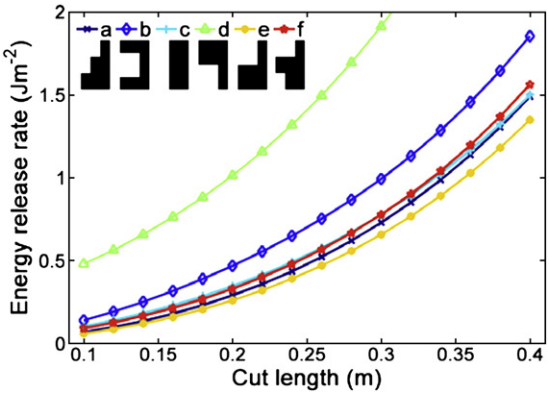

Fig. 3. Energy release rate vs. cut length for various slab layer configurations (profiles a to f).

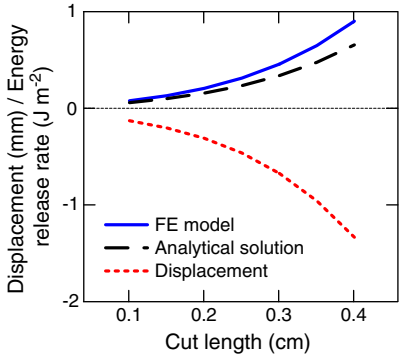

Fig. 4. Comparison of analytical solution with numerical solution (FE model). Energy release rate and maximal (slope normal) displacement vs. cut length for standard geometry of PST test (slope angle $\alpha = 30°$, block length $s = 1.2$ m, block width $d = 0.3$ m, gap width $\Delta_{gap} = 0.003$ m, slab thickness $H = 0.3$ m, thickness of base layer $h_{base} = 0.4$ m) with a relatively stiff base layer ($E_{base} = 60$ MPa, $\rho_{base} = 380$ kg m^{-3}) compared to the slab layer ($E_{slab} = 3$ MPa, $\rho_{slab} = 240$ kg m^{-3}).

3.2. Field measurements

The weak layers we tested in the field mainly consisted of rounding faceted particles (FCxr) and faceted crystals (FC); typical crystal size was 1–2 mm. Slab thickness (measured slope normal) ranged from 25 to 43 cm with a median of 37 cm; slope angle was between 20 and 33° with a median of 30°. Mean slab density varied between 170 and 280 kg m^{-3} (median: 250 kg m^{-3}). With 28 cm the median critical crack length was smaller than the median slab thickness (Tables 1 and 3).

Deriving the elastic properties of the slab from the snow micropenetrometer measurements (SMP method) yielded values of the modulus ranging from 1.8 to 12 MPa with a median value $E_{slab} =$ 3.4 MPa (Table 3). These values were used to calculate the critical energy release rate for each of the 149 PSTs with its specific geometry and material properties. The resulting fracture energies ranged between 0.28 and 2.2 J m^{-2} with a median value of 1 J m^{-2} (Table 3, Fig. 5). These values were highly correlated with the critical cut length suggesting that slab properties were fairly similar. In most cases the critical cut length was similar to the slab thickness ($r_c/H \cong 0.9$).

Using average slab properties and applying the analytical solution yielded considerably lower fracture energies with a median value of about 0.15 J m^{-2} — as expected from the results shown above.

Our data of weak layer fracture energy (Fig. 5) do not show any clear trends in regard to weak layer characteristics. There is a slight, but statistically not significant, trend for larger values of the specific fracture energy with larger grain size. On the three days when the specific fracture energy was lowest (8, 15 and 16 February 2010), the rutschblock score was 3 or less, whereas on the other days with mainly higher values of the specific fracture energy the rutschblock score was 5. Obviously, the dataset is too small for any firm conclusions on this apparent trend.

4. Discussion

The values of weak layer fracture energy obtained with the FE model using the SMP method to estimate the moduli were about an order of magnitude larger than the single value reported by Sigrist and Schweizer (2007). The difference seems – in part – to be related to the fact that Sigrist (2006) adjusted his SMP micro-modulus to values of the modulus obtained with a dynamic measuring method at 100 Hz. Accordingly, for our median slab density (250 kg m^{-3}) a modulus of about 21 MPa would result. Our median slab stiffness was 3.4 MPa with a slab density higher than the slab density reported by Sigrist and Schweizer (2007). Obviously, using smaller values for the modulus increases the specific fracture energy as more mechanical energy is available due to increased bending. However, the different results for the specific fracture energy do not solely stem from the different material properties but are also related to the geometry of the FE model. We used a thick basal layer in our FE model so that the energy release rate and hence the specific fracture energy substantially increased compared to the results obtained with the FE geometry used by Sigrist and Schweizer (2007). Therefore, we do not think that the difference between our results and those of Sigrist and Schweizer (2007) can be attributed solely to a rate effect — as is known to exist for snow strength (e.g. Schweizer et al., 2003).

On 12 March 2010 we also recorded a video sequence of one fracture test. This enabled us to obtain independent verification data using the PTV method. The mean slab stiffness determined with the

Table 3
Summary of propagation saw tests: measurements (average slab thickness H, average slab density r_{slab}, average critical cut length r_c), observations (type of weak layer) and results (average slab modulus E_{slab}, critical energy release rate or specific fracture energy w_f).

Date	Location	N	H (cm)	ρ_{slab} (kg m^{-3})	E_{slab} (MPa)	Weak layer (mm)	r_c (cm)	w_f (J m^{-2})
8 Feb 2010	Chilcherberg	19	34 ± 10	170	1.8	FCxr, 1–2	17 ± 5	0.4 ± 0.4
15 Feb 2010	Hüreli	15	24 ± 1	270	3.2	FC, 1–1.5	26 ± 7	0.7 ± 0.4
16 Feb 2010	Steintälli	18	35 ± 3	180	2.0	FC(FCxr), 0.75–1.5	24 ± 3	0.6 ± 0.3
25 Feb 2010	Steintälli	18	30 ± 3	250	3.7	FCxr, 1.5–3	29 ± 4	1.7 ± 1.1
3 Mar 2010	Dorfberg	14	33 ± 3	280	12.1	FCxr(FC)	43 ± 7	2.2 ± 2.2
8 Mar 2010	Vorder Latschüel	18	40 ± 7	260	4.2	FC,1–2	36 ± 5	1.8 ± 1.0
12 Mar 2010	Chilcherberg	23	38 ± 8	260	3.8	FCxr, 1.5–2.5	35 ± 3	2.1 ± 0.8
18 Mar 2010	Mittelgrat	24	28 ± 5	210	2.6	FCxr(DH), 1–2	27 ± 4	0.8 ± 0.3

For slab thickness H (slope normal), critical cut length r_c and specific fracture energy w_f the mean and standard deviation are given for the number of PST's (N). The weak layer is described as grain type and size according to Fierz et al. (2009).

SMP method was 3.8 ± 0.8 MPa while with the PTV method the mean elastic modulus of the slab was determined to 1.5 MPa (van Herwijnen and Heierli, 2010a). The specific fracture energy for the weak layer determined using the PTV method was 1.4 J m^{-2}, whereas the SMP-FE method yielded a mean value of 2.1 ± 0.8 J m^{-2} (N = 23). The values of the modulus obtained with the SMP and the PTV methods were in reasonable agreement. The elastic modulus obtained with the PTV method was somewhat lower than that obtained with the SMP method. However, the order of magnitude was similar, suggesting that the values used by Sigrist and Schweizer (2007) were too high. Furthermore, the weak layer fracture energies obtained with the two independent methods were in good agreement.

Given the material properties of snow, it makes sense to use effective rather than purely elastic moduli. Snow does not behave like a purely elastic material, except for very small deformations or very short times (e.g. Camponovo and Schweizer, 2001). The time used to perform a propagation saw test or an SMP measurement is on the order of seconds. The SMP probe runs at 20 mm s^{-1}, whereas the cutting speed in a PST is on the order of 50 mm s^{-1}. It is therefore likely that the snow exhibits some non-elastic behavior. Values of the effective modulus of 1 MPa as obtained in our study are in agreement with previous measurements obtained with torsional shear experiments at 1 Hz (Camponovo and Schweizer, 2001).

On all field days, the slab layers contained some hard layers or crusts. Such stiff layers can substantially reduce the amount of bending so that one would expect the analytical solution which uses an average modulus to yield higher specific fracture energy than obtained with the FE method. Nevertheless, the values calculated with the analytical solution were slightly smaller. These discrepancies likely follow from the assumptions made to derive the analytical solution (Heierli, 2008). In the analytical solution the substratum, as well as the weak layer, are assumed to be rigid. Deformation of the slab is therefore contained in the section of the beam which is not supported anymore (i.e. up to the crack tip). The FE simulations, as well as the measurements presented in van Herwijnen and Heierli (2010a) clearly show that the slab deforms ahead of the crack tip, up to a distance roughly equal to the crack length. Therefore, the increased deformation results in more energy being released and a higher specific fracture energy for the weak layer is obtained. Furthermore, the Timoshenko approximation assumes that $r_c \gg H$, a condition which was not fulfilled in our experiments. Obviously, the assumption of a rigid substrate can be relaxed under certain conditions ($r_c \ll H$) and the so-called elastic mismatch between slab and substratum can be taken into account (Heierli, 2008; Hutchinson and Suo, 1992). However, we have not attempted to do so.

As we only tested a few weak layers, mainly consisting of faceted crystals, we cannot make any conclusion on the dependence of the specific fracture energy on weak layer properties. We only observed that weak layers with low specific fracture energy tended to consist of relatively small faceted grains and failed at low rutschblock scores, and vice versa.

5. Conclusions

We have performed about 150 propagation saw tests to obtain the weak layer fracture energy from measurements of critical crack length, slab thickness and density. Slab stiffness, required to calculate the energy release rate, was estimated from SMP measurements.

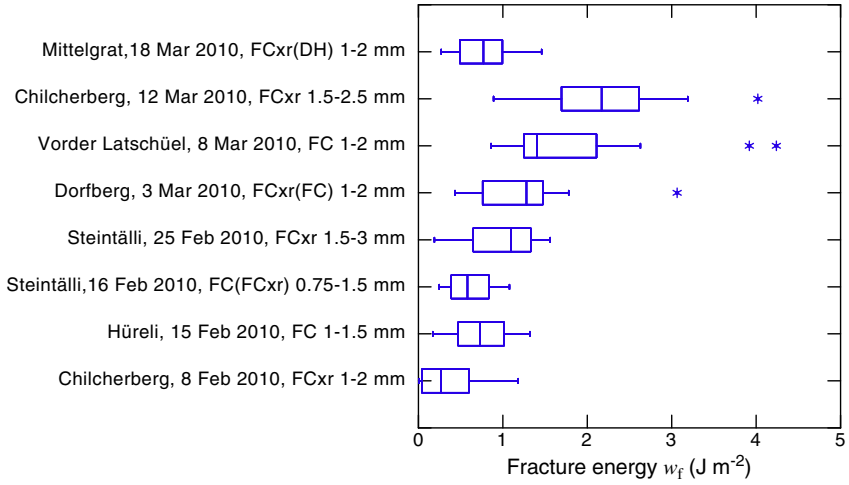

Fig. 5. Distribution of weak layer fracture energy w_f calculated with the SMP-FE method for each of the eight field days. Also given is weak layer grain type and size (N = 144, 5 extreme outliers with w_f > 5 J m^{-2} are not shown). Boxes span the interquartile range from 1st to 3rd quartile with a horizontal line showing the median. Whiskers show the range of observed values that fall within 1.5 times the interquartile range above and below the interquartile range; asterisks denote remaining outliers.

The specific fracture energies calculated with the FE method for our weak layer/slab configurations were on the order of $1\,J\,m^{-2}$. These values are large compared to the only previously published value based on field measurements of $0.07\,J\,m^{-2}$. The reason for the discrepancy is not entirely clear; it largely – but not solely – stems from the lower values of the E modulus we used. Using the input data previously published by Sigrist and Schweizer (2007) we were able to reproduce their low value. More important, with the PTV method, an independent approach, a similarly high value of the fracture energy for the weak layer tested on 12 March 2010 was obtained. Accordingly, we are confident that the values of weak layer fracture energy we calculated are realistic.

The present dataset of weak layer fracture energy is not sufficiently diverse in regard to weak layer properties for any conclusions on the relation between specific fracture energy and weak layer properties. Our preliminary results suggest that there might be a relation between weak layer fracture energy and rutschblock score.

As shown by the FE simulations with different slab configurations the slab layering strongly affects the critical cut length for a given weak layer fracture energy. Typically, relatively large critical cut lengths are observed with stiff slabs — independently of the weak layer fracture energy. The critical cut length integrates the slab properties as well as the weak layer properties. As pointed out by Sigrist and Schweizer (2007) the energy that has to be exceeded to fracture a weak layer depends on the material properties of the weak layer, whereas the energy that is available for crack propagation depends initially (and mainly) on the material properties of the overlying slab and eventually on the slope normal collapse height of the weak layer.

For the future it will be essential to perform more measurements in order to obtain a comprehensive dataset of weak layer fracture energy. This will allow numerical snow cover models to provide critical cut lengths for simulated weak layer/slab configurations as a measure of instability.

Acknowledgments

We would like to thank Susanna Hoinkes, Christoph Mitterer and Jake Turner for help with the field work and Joachim Heierli for his contribution to the PTV method. We are grateful for the comments by two anonymous reviewers that helped to improve the paper. We are also indebted to Joachim Heierli for pointing out some errors in the analytical solution we initially used. Part of this work was performed while Alec van Herwijnen was at Montana State University supported by a fellowship for advanced researchers from the Swiss National Science Foundation (grant PA00P2_131462).

References

Anderson, T.L., 1995. Fracture mechanics: fundamentals and applications. CRC Press, Boca Raton, U.S.A.. 688 pp.

Camponovo, C., Schweizer, J., 2001. Rheological measurements of the viscoelastic properties of snow. Annals of Glaciology 32, 44–50.

Fierz, C., Armstrong, R.L., Durand, Y., Etchevers, P., Greene, E., McClung, D.M., Nishimura, K., Satyawali, P.K., Sokratov, S.A., 2009. The international classification for seasonal snow on the ground. HP-VII Technical Documents in Hydrology, 83. UNESCO-IHP, Paris, France. 90 pp.

Gauthier, D., Jamieson, B., 2010. On the Sustainability and Arrest of Weak Layer Fracture in Whumpfs and Avalanches, International Snow Science Workshop ISSW, Lake Tahoe CA, U.S.A., 17–22 October 2010, pp. 224–231.

Gauthier, D., Jamieson, J.B., 2006. Towards a field test for fracture propagation propensity in weak snowpack layers. Journal of Glaciology 52 (176), 164–168.

Gauthier, D.M., 2007. A practical field test for fracture propagation and arrest in weak snowpack layers in relation to slab avalanche release. Ph.D. Thesis, University of Calgary, Calgary AB, Canada, 302 pp.

Habermann, M., Schweizer, J., Jamieson, J.B., 2008. Influence of snowpack layering on human-triggered snow slab avalanche release. Cold Regions Science and Technology 54 (3), 176–182.

Heierli, J., 2008. Anticrack model for slab avalanche release. Ph.D. Thesis, University of Karlsruhe, Karlsruhe, Germany, 102 pp.

Heierli, J., Gumbsch, P., Zaiser, M., 2008. Anticrack nucleation as triggering mechanism for snow slab avalanches. Science 321 (5886), 240–243.

Heierli, J., Zaiser, M., 2006. An analytical model for fracture nucleation in collapsible stratifications. Geophysical Research Letters 33, L06501. doi:10.1029/2005GL025311.

Hutchinson, J.W., Suo, Z., 1992. Mixed-mode cracking in layered materials. In: Hutchinson, J.W., Wu, T.Y. (Eds.), Advances in Applied Mechanics. Academic Press, London, Advances in Applied Mechanics, pp. 63–191.

Jamieson, J.B., Schweizer, J., 2000. Texture and strength changes of buried surface hoar layers with implications for dry snow-slab avalanche release. Journal of Glaciology 46 (152), 151–160.

Johnson, J.B., Schneebeli, M., 1999. Characterizing the microstructural and micromechanical properties of snow. Cold Regions Science and Technology 30 (1–3), 91–100.

Kirchner, H.O.K., Michot, G., Suzuki, T., 2000. Fracture toughness of snow in tension. Philosophical Magazine A 80 (5), 1265–1272.

Kronholm, K., 2004. Spatial variability of snow mechanical properties with regard to avalanche formation. Ph.D. Thesis, University of Zurich, Zurich, Switzerland, 192 pp.

Marshall, H.-P., Johnson, J.B., 2009. Accurate inversion of high-resolution snow penetrometer signals for microstructural and micromechanical properties. Journal of Geophysical Research 114 (F4), F04016.

McClung, D.M., 1979. Shear fracture precipitated by strain softening as a mechanism of dry slab avalanche release. Journal of Geophysical Research 84 (87), 3519–3526.

McClung, D.M., 1981. Fracture mechanical models of dry slab avalanche release. Journal of Geophysical Research 86 (B11), 10783–10790.

McClung, D.M., 2007. Fracture energy applicable to dry snow slab avalanche release. Geophysical Research Letters 34 (2), L02503.

Mellor, M., 1975. A review of basic snow mechanics. Symposium at Grindelwald 1974 - Snow Mechanics, IAHS Publ, 114. Int. Assoc. Hydrol. Sci, Wallingford, U.K, pp. 251–291.

Scapozza, C., 2004. Entwicklung eines dichte- und temperaturabhängigen Stoffgesetzes zur Beschreibung des visko-elastischen Verhaltens von Schnee. Ph.D. Thesis, ETH Zurich, Zurich, Switzerland, 250 pp.

Schneebeli, M., Johnson, J.B., 1998. A constant-speed penetrometer for high-resolution snow stratigraphy. Annals of Glaciology 26, 107–111.

Schweizer, J., Lütschg, M., 2001. Characteristics of human-triggered avalanches. Cold Regions Science and Technology 33 (2–3), 147–162.

Schweizer, J., Jamieson, J.B., Schneebeli, M., 2003. Snow avalanche formation. Reviews of Geophysics 41 (4), 1016. doi:10.1029/2002RG000123.

Schweizer, J., Michot, G., Kirchner, H.O.K., 2004. On the fracture toughness of snow. Annals of Glaciology 38, 1–8.

Sigrist, C., 2006. Measurement of fracture mechanical properties of snow and application to dry snow slab avalanche release. Ph.D. Thesis, ETH Zurich, Zurich, Switzerland, 139 pp.

Sigrist, C., Schweizer, J., 2007. Critical energy release rates of weak snowpack layers determined in field experiments. Geophysical Research Letters 34 (3), L03502. doi:10.1029/2006GL028576.

Sigrist, C., Schweizer, J., Schindler, H.J., Dual, J., 2006. The energy release rate of mode II fractures in layered snow samples. International Journal of Fracture 139 (3–4), 461–475.

Sturm, M., Johnson, J.B., Holmgren, J.A., 2004. Variations in the mechanical properties of arctic and subarctic snow at local (1-m) to regional (100-km) scales, Proceedings ISSMA-2004, International Symposium on Snow Monitoring and Avalanches, Manali, India, 12–16 April 2004. Snow and Avalanche Study Establishment, India. pp. 233–238.

van Herwijnen, A., Heierli, J., 2010a. A field method for measuring slab stiffness and weak layer fracture energy. International Snow Science Workshop ISSW, Lake Tahoe CA, U.S.A., 17–22 October 2010, pp. 232–237.

van Herwijnen, A., Heierli, J., 2010b. In-situ measurement of the mechanical energy associated with crack growth in weak snowpack layers and determination of the fracture energy. Geophysical Research Abstracts 12, 11743.

van Herwijnen, A., Schweizer, J., Heierli, J., 2010. Measurement of the deformation field associated with fracture propagation in weak snowpack layers. Journal of Geophysical Research 115, F03042. doi:10.1029/2009JF001515.